Memo version 4.0

BESIII Analysis Memo

DocDB-697

BAM-336

May 14, 2019

Study of $\psi(3686) \to \Lambda\bar{\Lambda}\omega$

Honghong Zhang[a,b], Yunchi chen [a,b], and Beijing Liu [b], and Daihui Wei [a]

[a]*Guang Xi Normal University*
[b]*Institute of High Energy Physics*

Internal Referee Committee

Ref1 Jianbin Jiao (Chair)[d], Ref2 Ismail Uman[e], and Ref3 Fritz-Herbert Heinsius[f]

[d]*Shan Dong University*
[e]*TACPF*
[f]*Bochum*

DocDB : http://docbes3.ihep.ac.cn/cgi-bin/DocDB/ShowDocument?docid=697

Hypernews : http://hnbes3.ihep.ac.cn/HyperNews/get/paper336.html

Abstract

Based on 4.48×10^8 $\psi(3686)$ events collected with BESIII detector at BEPCII, we present the measurement of $\psi(3686) \to \Lambda\bar{\Lambda}\omega$, which is observed for the first time. The branching fraction is measured to be $(3.42 \pm 0.34(stat.) \pm 0.31(syst.)) \times 10^{-5}$. There is no evidence of any Λ^* in both and mass distributions. However a 2-dimesional fit to the Dalitz plot of $\psi(3686) \to \Lambda\bar{\Lambda}\omega$ gives a mass of 2.001 ± 0.007 GeV/c^2 and width is 0.036 ± 0.014 GeV/c^2 with the significance of 3.3σ. The corresponding upper limit branching fraction of B($\psi(3686) \to \Lambda\bar{\Lambda}^*/\bar{\Lambda}\Lambda^* \to \Lambda\bar{\Lambda}\omega$) is estimated to be 1.93×10^{-5} at 90% confidence level.

Contents

1 Introduction

Hadron spectroscopy is a unique way to access quantum chromo dynamics(QCD). Given many recent processes, our present baryon spectroscopy is still in its infancy[1]. Many fundamental issues in baryon spectroscopy are still not well understood[2]. Charmonium decays provide an excellent place for studying excited nucleons and hyperons $-N^*$, Λ^*, Σ^* and Ξ^*[3].

Many Λ resonances are predicted by quark model, but there are some Λ resonances which evidence of existence is poor[4]. The isospin conserving decay mode of $\psi(3686) \to X\Lambda$, $X \to \bar{\Lambda}\omega$ provides a good hunting ground for the potential Λ excitations.

Using 4.48×10^8 $\psi(3686)$ events collected at BESIII, we measure the branching fractions of $\psi(3686) \to \Lambda\bar{\Lambda}\omega$ which is observed for the first time and would guide us to study more exclusive channels and search for intermediate states of $\Lambda^* \to \Lambda\omega$ or $\bar{\Lambda}^* \to \bar{\Lambda}\omega$.

2 BESII detector and Monte Carlo simulation

The Beijing Electron Positron Collider II (BEPCII is a double-ring e^+e^- collider designed to operate in the τ-charm region with an achieved luminosity of 10^{33} $cm^{-2}s^{-1}$ at the center-of-mass energy of 3.686 GeV. The BESIII detector has a geometrical acceptance of 93% of 4π immersed in a magnetic filed of 1.0 T[5]. The BESIII detector is composed of a helium-based main drift chamber (MDC), a plastic scintillator Time-of-flight system (TOF), a CsI (Tl) electromagnetic calorimeter (EMC) and a muon system (MUC) made of resistive plate chambers (RPC). The charged particle momentum resolution is 0.5% at 1 GeV/c^2 and the energy-loss (dE/dx) resolution is better than 6%. The time resolution of TOF is 80 ps (110 ps) in the barrel (end-caps) detectors. The photon energy resolution is 2.5% (5%) at 1.0 GeV in the barrel (end-caps) of the EMC. The spatial resolution in the MUC is better than 2 cm.

A GEANT4-based[6] Monte Carlo (MC) simulation package is used to determine the detection efficiency, optimize event criteria and estimate backgrounds. The $\psi(3686)$ resonance is generated by KKMC[7], where the known decay modes are generated by EvtGen[8] with BF(Branching fraction) set to the world average values[4] and the remaining decays are generated by Lundcharm model[9]. The analysis is based on a sample of 4.48×10^8 $\psi(3686)$ events collected with the BESIII detector operating at the BEPCII collider in 2009 and 2012, and the software framework used for the data analysis is BESIII Offline Software System (Boss). The BOSS version is 6.6.4.p03. An inclusive MC sample of 5.06×10^8 $\psi(3686)$ events is used to investigate possible background. And an exclusive MC samples of 1.0×10^6 $\psi(3686)$ events is generated to optimize the selection criteria and determine the corresponding selection efficiencies. Tab 1 shows the decay card we use to generate the decay channel of $\psi(3686) \to \Lambda\bar{\Lambda}\omega$.

```
Decay psi(2s)
  1.000 anti-Lambda0 Lambda0 omega PHSP;
Enddecay
Decay Lambda0
  1.00 p+ pi- HypWK;
Enddecay
Decay anti-Lambda0
  1.00 anti-p- pi+ HypWK;
Enddecay
Decay omega
  1.000 pi+ pi- pi0 OMEGA_DALITZ;
Enddecay
Decay pi0
  1.000 gamma gamma PHSP;
Enddecay
End
```

Table 1: The decay card of Exclusive MC

3 Event selection

The decay $\psi(3686) \to \Lambda\bar{\Lambda}\omega$ is reconstructed from cascade decays $\Lambda \to p\pi^-$, $\bar{\Lambda} \to \bar{p}\pi^+$, $\omega \to \pi^+\pi^-\pi^0$ and $\pi^0 \to \gamma\gamma$.

Charged-particle tracks in the polar angle range $|\cos\theta| < 0.93$ are reconstructed hits from the MDC. For the pions decay from ω, tracks with their points of closest approach to the beamline within 10 cm of the interaction point in the beam direction, and within 1 cm in the plane perpendicular to the beam are selected. The number of charged tracks is required to be 6, the net charge of the event is 0. TOF and dE/dx information are combined to determine particle identification confidence levels for π, K and p hypotheses; and the particle type with highest confidence level is assigned to each track. To identify a track is a pion, it is required $Prob(\pi) > Prob(p)$ and $Prob(\pi) > Prob(K)$. The π^+ *and* π^- decay from ω are required to be identified. There is no PID(particle identification identify) requirement on the proton and pion decay from Λ and $\bar{\Lambda}$. The decay product of Λ ($\bar{\Lambda}$) with larger Prob(p) is assigned as proton(antiproton).

We loop all positive and negative charged tracks through second vertex fit to reconstruct $\Lambda\bar{\Lambda}$ and select a pair of Λ and $\bar{\Lambda}$ with the minimal value of $((m_\Lambda - M_\Lambda)^2 + (m_{\bar{\Lambda}} - M_{\bar{\Lambda}})^2)$ in all combinations, where M_Λ and $M_{\bar{\Lambda}}$ are the mass of reconstructed Λ and $\bar{\Lambda}$, m_Λ and $m_{\bar{\Lambda}}$ are the mass of Λ and $\bar{\Lambda}$ in PDG. There's no further requirement on the χ^2 and decay length of the seconde vertex fit for the $\Lambda/\bar{\Lambda}$ candidate.

Photon candidates are reconstructed by clustering signals in EMC crystals. The photon candidates are required to be in the barrel region($|\cos\theta| < 0.8$) of the EMC with at least 25 MeV energy deposition, or in the endcaps region ($0.8 < |\cos\theta| < 0.92$) with at least 50 MeV energy deposition, where θ is the polar angle of the shower. The timing obtained from the EMC is required to be $0 \le t_{EMC} \le 700$ ns to

suppress electronic noise and energy depositions that are unrelated to the event. To suppress showers generated by charged particles, the photon candidates are furthermore required to be separated by an angle larger than 10° degree and larger than 30° from the proton and anti-proton, respectively. And there are no less than 2 photons with the requirements specified above.

π^0 candidates are selected from photon pairs, the selected $\gamma\gamma$ combinations are subjected to a one constraint (1C) kinematic fit under the $\pi^0 \to \gamma\gamma$ hypotheses, and the χ^2 of the 1C kinematic fit is required to be less 25.

We perform a 5C (five constraint) kinematic fit with the $\psi(3686) \to \Lambda\bar{\Lambda}\pi^+\pi^-\pi^0$ hypothesis with $\gamma\gamma$ constrained to π^0 decay. If there is more than one candidates, the combination with the smallest χ^2 will be selected.

After the optimization with $\frac{s}{\sqrt{s+b}}$(s denotes the events number of signal MC, and s + b is the total events number of data), the χ^2 of 5C kinematic fit is required to be less than 40 in this analysis, it is shown in the Fig. 1 .

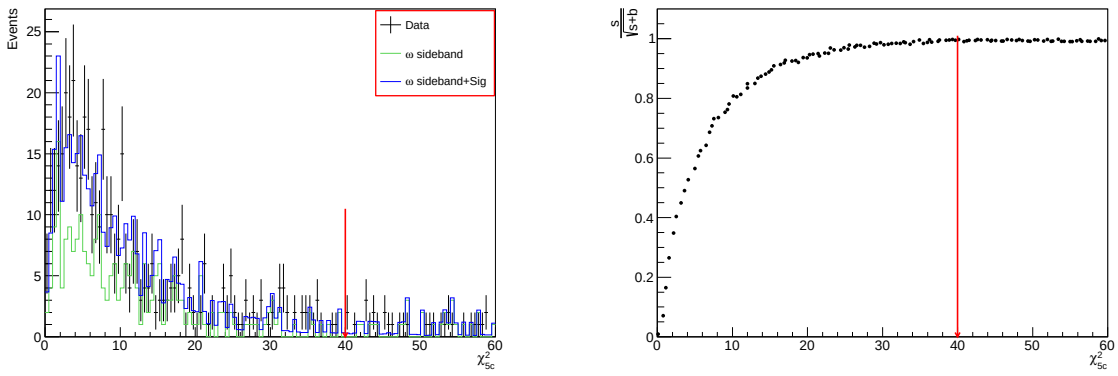

(a) (b)

Figure 1: (a) shows the χ^2 5C kinematic fit. The dots with error bars are from $\psi(3686)$ data, green histogram shows the normalized ω sideband background, blue histogram shows the normalized ω sideband background add the normalized $\psi(3686) \to \Lambda\bar{\Lambda}\omega$ exclusive MC phase space. (b) shows the $\frac{s}{\sqrt{s+b}}$ versus χ^2_{5C}

Invariant mass distributions of $p\pi^-$ and $\bar{p}\pi^+$ are shown in Fig. 2 (a) and Fig. 2 (b), where obvious Λ or $\bar{\Lambda}$ signal can be seen. $\Lambda(\bar{\Lambda})$ candidates are selected by requiring $|M_{p\pi^-(\bar{p}\pi^+)} - m_{\Lambda(\bar{\Lambda})}| < 5\ MeV/c^2$, where $M_{p\pi^-(\bar{p}\pi^+)}$ is the invariant mass of $p\pi^-(\bar{p}\pi^+)$ and $m_{\Lambda(\bar{\Lambda})}$ is the nominal mass of $\Lambda(\bar{\Lambda})$ from PDG[4]. Fig. 3 (a) and Fig. 3 (b) show the decay length of Λ and $\bar{\Lambda}$, respectively. And Fig. 4 (a) shows the scatter diagram of $M_{p\pi^-}$ versus $M_{\bar{p}\pi^+}$ from data.

The recoil mass of the system recoiling against $\pi^+\pi^-$ is shown in Fig. 4 (b), where an obvious J/ψ structure can be seen. Backgrounds from $\psi(3686) \to\ p\bar{p}J/\psi$ are rejected $|M^{rec}_{\pi^+\pi^-} - m_{J/\psi}| > 30\ MeV/c^2$,

$M^{rec}_{\pi^+\pi^-}$ is the recoil mass of the system recoiling against $\pi^+\pi^-$ and $m_{J/\psi}$ is the nominal mass of J/ψ.

In the process of searching for $\Lambda^*/\bar{\Lambda}^*$, ω candidates are selected by requiring $|M_{\pi^+\pi^-\pi^0} - m_\omega| < 30\ MeV/c^2$, $M_{\pi^+\pi^-\pi^0}$ is the invariant mass of $\pi^+\pi^-\pi^0$ and m_ω is the the nominal mass of ω. Invariant mass distribution of $\pi^+\pi^-\pi^0$ is shown in Fig. 5 (a).

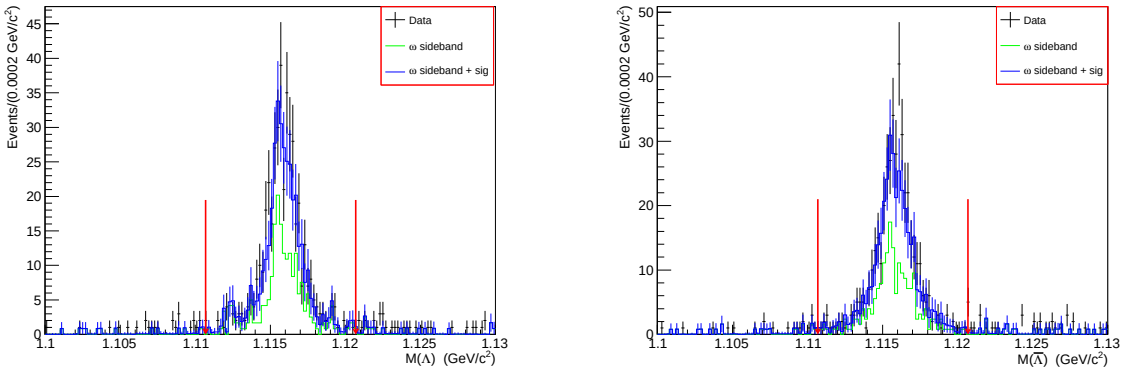

(a) (b)

Figure 2: (a) (b) shows invariant mass distribution of Λ and $\bar{\Lambda}$,respectively. The dots with error bars are from $\psi(3686)$ data, green histogram shows the background estimated with the ω sideband, blue histogram shows the ω sideband background add phase space background.

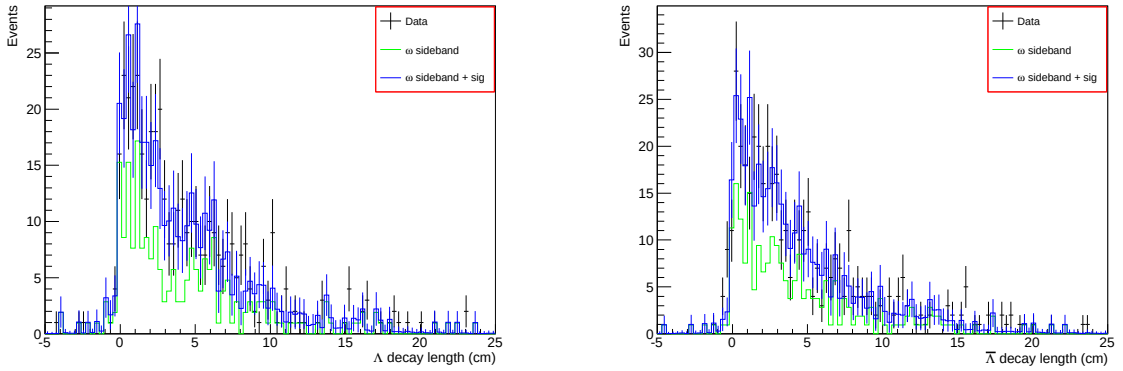

(a) (b)

Figure 3: (a)(b) shows the decay length of Λ and $\bar{\Lambda}$, respectively. The dots with error bars are from $\psi(3686)$ data, green histogram shows the background estimated with the ω sideband, blue histogram shows the ω sideband background add phase space background.

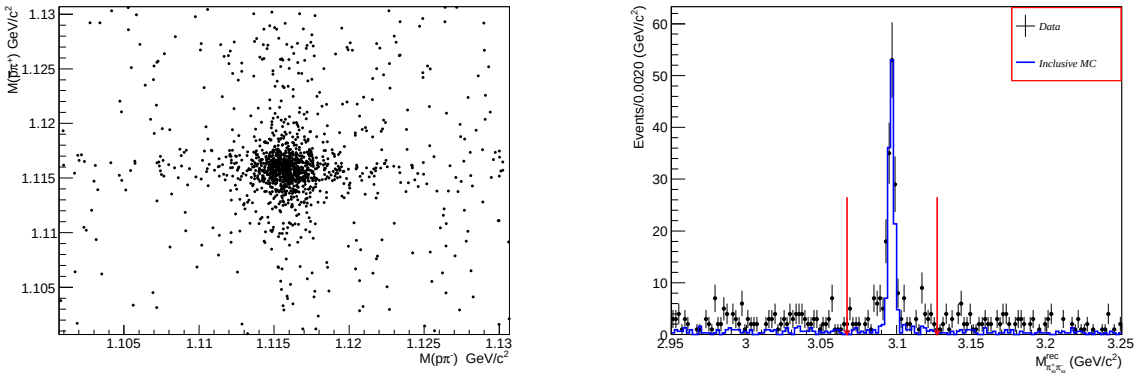

(*a*) (*b*)

Figure 4: (a) shows the scatter diagram of $M_{p\pi^-}$ versus $M_{\bar{p}\pi^+}$ from data. (b) shows the recoil mass of the system recoiling against $\pi^+\pi^-$, dots with error bars are from $\psi(3686)$ data, blue histogram comes from Inclusive MC.

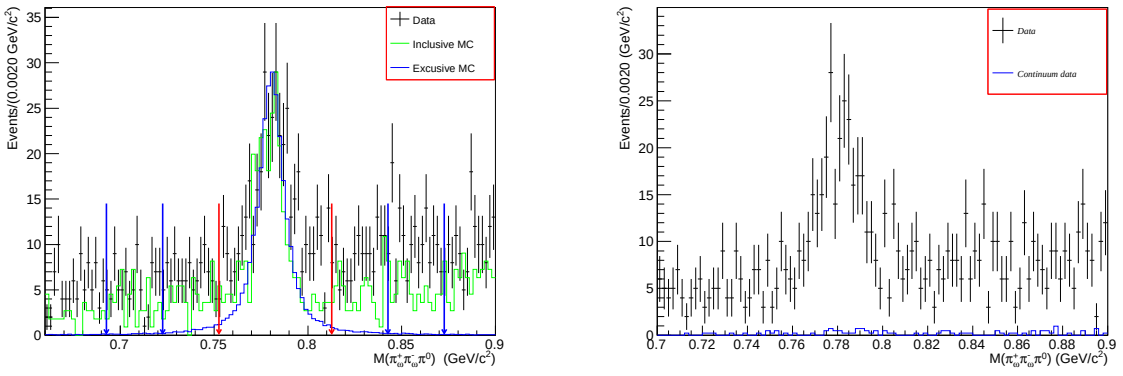

(*a*) (*b*)

Figure 5: The invariant mass distribution of $\pi^+\pi^-\pi^0$ (a) dots with error bars are from $\psi(3686)$ data, green histogram comes from Inclusive MC, blue histogram comes from phase space and the blue arrow is the ω sideband region, the red arrow is the ω signal region. (b) the dots with error bars are from $\psi(3686)$ data, blue histogram shows the background estimated with the continuum data at 3.773GeV data after the normalization

4 Background analysis

No.	decay chain	final states	iTopo	nEvt	nTot
0	$\psi(3686) \to \bar{\Lambda}\omega\Lambda$, $\bar{\Lambda} \to \bar{p}\pi^+$, $\omega \to \pi^-\pi^0\pi^+$, $\Lambda \to \pi^- p$,	$\psi(3686) \to \gamma\gamma p\pi^+\pi^+\pi^-\pi^-\bar{p}$	1	226	226
1	$\psi(3686) \to \bar{\Sigma}^{*+}\pi^0\Sigma^{*-}$, $\bar{\Sigma}^{*+} \to \bar{\Lambda}\pi^+$, $\Sigma^{*-} \to \pi^-\Lambda$, $\bar{\Lambda} \to \bar{p}\pi^+$, $\Lambda \to \pi^- p$,	$\psi(3686) \to \gamma\gamma p\pi^+\pi^+\pi^-\pi^-\bar{p}$	0	16	242
2	$\psi(3686) \to \bar{\Sigma}^{*-}\pi^0\Sigma^{*+}$, $\bar{\Sigma}^{*-} \to \bar{\Lambda}\pi^-$, $\Sigma^{*+} \to \pi^+\Lambda$, $\bar{\Lambda} \to \bar{p}\pi^+$, $\Lambda \to \pi^- p$,	$\psi(3686) \to \gamma\gamma p\pi^+\pi^+\pi^-\pi^-\bar{p}$	10	7	249
3	$\psi(3686) \to \pi^-\pi^+ J/\psi$, $J/\psi \to \bar{\Delta}^{++}\pi^0\Delta^{++}$, $\bar{\Delta}^{++} \to \bar{p}\pi^-$, $\Delta^{++} \to \pi^+ p$,	$\psi(3686) \to \gamma\gamma p\pi^+\pi^+\pi^-\pi^-\bar{p}$	13	7	256
4	$\psi(3686) \to \bar{\Xi}^+\pi^0\Xi^-$, $\bar{\Xi}^+ \to \bar{\Lambda}\pi^+$, $\Xi^- \to \pi^-\Lambda$, $\bar{\Lambda} \to \bar{p}\pi^+$, $\Lambda \to \pi^- p$,	$\psi(3686) \to \gamma\gamma p\pi^+\pi^+\pi^-\pi^-\bar{p}$	29	7	263
5	$\psi(3686) \to \gamma\chi_{c1}$, $\chi_{c1} \to \bar{\Sigma}^{*-}\pi^+\Sigma^0$, $\bar{\Sigma}^{*-} \to \bar{\Lambda}\pi^-$, $\Sigma^0 \to \gamma\Lambda$, $\Lambda \to \pi^- p$, $\bar{\Lambda} \to \bar{p}\pi^+$,	$\psi(3686) \to \gamma\gamma p\pi^+\pi^+\pi^-\pi^-\bar{p}$	14	4	267
6	$\psi(3686) \to \bar{\Xi}^0\pi^+\Xi^-$, $\bar{\Xi}^0 \to \bar{\Lambda}\pi^0$, $\Xi^- \to \pi^-\Lambda$, $\bar{\Lambda} \to \bar{p}\pi^+$, $\Lambda \to \pi^- p$,	$\psi(3686) \to \gamma\gamma p\pi^+\pi^+\pi^-\pi^-\bar{p}$	17	4	271
7	$\psi(3686) \to \bar{\Xi}^+\pi^-\Xi^0$, $\bar{\Xi}^+ \to \bar{\Lambda}\pi^+$, $\Xi^0 \to \pi^0\Lambda$, $\bar{\Lambda} \to \bar{p}\pi^+$, $\Lambda \to \pi^- p$,	$\psi(3686) \to \gamma\gamma p\pi^+\pi^+\pi^-\pi^-\bar{p}$	28	4	275
8	$\psi(3686) \to \pi^-\pi^+ J/\psi$, $J/\psi \to \bar{p}\omega p$, $\omega \to \pi^-\pi^0\pi^+$,	$\psi(3686) \to \gamma\gamma p\pi^+\pi^+\pi^-\pi^-\bar{p}$	3	4	279
9	$\psi(3686) \to \gamma\chi_{c2}$, $\chi_{c2} \to \Sigma^0\pi^-\Sigma^{*+}$, $\Sigma^0 \to \bar{\Lambda}\gamma$, $\Sigma^{*+} \to \pi^+\Lambda$, $\Lambda \to \pi^- p$, $\bar{\Lambda} \to \bar{p}\pi^+$,	$\psi(3686) \to \gamma\gamma p\pi^+\pi^+\pi^-\pi^-\bar{p}$	26	3	282
10	$\psi(3686) \to \pi^-\pi^+ J/\psi$, $J/\psi \to \bar{p}n\pi^-\pi^0\pi^+ p$,	$\psi(3686) \to \gamma\gamma p\pi^+\pi^+\pi^-\pi^-\bar{p}$	11	3	285
11	$\psi(3686) \to \pi^-\pi^+ J/\psi$, $J/\psi \to \bar{\Sigma}^{*-}\Sigma^+$, $\bar{\Sigma}^{*-} \to \bar{\Lambda}\pi^-$, $\Sigma^+ \to \pi^0 p$, $\bar{\Lambda} \to \bar{p}\pi^+$,	$\psi(3686) \to \gamma\gamma p\pi^+\pi^+\pi^-\pi^-\bar{p}$	5	3	288
12	$\psi(3686) \to \pi^-\pi^+ J/\psi$, $J/\psi \to \bar{\Lambda}\pi^-\Sigma^+$, $\bar{\Lambda} \to \bar{p}\pi^+$, $\Sigma^+ \to \pi^0 p$,	$\psi(3686) \to \gamma\gamma p\pi^+\pi^+\pi^-\pi^-\bar{p}$	36	3	291
13	$\psi(3686) \to \gamma\chi_{c1}$, $\chi_{c1} \to \gamma J/\psi$, $J/\psi \to \bar{\Sigma}^{*-}\Sigma^{*+}$, $\bar{\Sigma}^{*-} \to \bar{\Lambda}\pi^-$, $\Sigma^{*+} \to \pi^+\Lambda$, $\Lambda \to \pi^- p$, $\bar{\Lambda} \to \bar{p}\pi^+$,	$\psi(3686) \to \gamma\gamma p\pi^+\pi^+\pi^-\pi^-\bar{p}$	12	2	293
14	$\psi(3686) \to \bar{\Sigma}^0\rho^0\Sigma^0$, $\bar{\Sigma}^0 \to \bar{\Lambda}\gamma$, $\rho^0 \to \pi^-\pi^+$, $\Sigma^0 \to \gamma\Lambda$, $\bar{\Lambda} \to \bar{p}\pi^+$, $\Lambda \to \pi^- p$,	$\psi(3686) \to \gamma\gamma p\pi^+\pi^+\pi^-\pi^-\bar{p}$	2	2	295
15	$\psi(3686) \to \bar{\Sigma}^{*0}\pi^+\Sigma^{*-}$, $\bar{\Sigma}^{*0} \to \bar{\Lambda}\pi^0$, $\Sigma^{*-} \to \pi^-\Lambda$, $\Lambda \to \pi^- p$, $\bar{\Lambda} \to \bar{p}\pi^+$,	$\psi(3686) \to \gamma\gamma p\pi^+\pi^+\pi^-\pi^-\bar{p}$	19	2	297
16	$\psi(3686) \to \gamma\chi_{c1}$, $\chi_{c1} \to \gamma J/\psi$, $J/\psi \to \bar{\Sigma}^{*+}\Sigma^{*-}$, $\bar{\Sigma}^{*+} \to \bar{\Lambda}\pi^+$, $\Sigma^{*-} \to \pi^-\Lambda$, $\Lambda \to \pi^- p$, $\bar{\Lambda} \to \bar{p}\pi^+$,	$\psi(3686) \to \gamma\gamma p\pi^+\pi^+\pi^-\pi^-\bar{p}$	30	2	299
17	$\psi(3686) \to \pi^-\pi^+ J/\psi$, $J/\psi \to \bar{\Sigma}^-\pi^+\Lambda$, $\bar{\Sigma}^- \to \bar{p}\pi^0$, $\Lambda \to \pi^- p$,	$\psi(3686) \to \gamma\gamma p\pi^+\pi^+\pi^-\pi^-\bar{p}$	23	2	301
18	$\psi(3686) \to \bar{\Sigma}^0\pi^-\pi^+\Sigma^0$, $\bar{\Sigma}^0 \to \bar{\Lambda}\gamma$, $\Sigma^0 \to \gamma\Lambda$, $\Lambda \to \pi^- p$, $\bar{\Lambda} \to \bar{p}\pi^+$,	$\psi(3686) \to \gamma\gamma p\pi^+\pi^+\pi^-\pi^-\bar{p}$	18	1	302
19	$\psi(3686) \to \bar{\Sigma}^{*-}\pi^+\Sigma^{*0}$, $\bar{\Sigma}^{*-} \to \bar{\Lambda}\pi^-$, $\Sigma^{*0} \to \pi^0\Lambda$, $\Lambda \to \pi^- p$, $\bar{\Lambda} \to \bar{p}\pi^+$,	$\psi(3686) \to \gamma\gamma p\pi^+\pi^+\pi^-\pi^-\bar{p}$	6	1	303
20	$\psi(3686) \to \pi^0 J/\psi$, $J/\psi \to \bar{\Sigma}^{*-}\Sigma^{*+}$, $\bar{\Sigma}^{*-} \to \bar{\Lambda}\pi^-$, $\Sigma^{*+} \to \pi^+\Lambda$, $\Lambda \to \pi^- p$, $\bar{\Lambda} \to \bar{p}\pi^+$,	$\psi(3686) \to \gamma\gamma p\pi^+\pi^+\pi^-\pi^-\bar{p}$	20	1	304
21	$\psi(3686) \to \gamma\chi_{c0}$, $\chi_{c0} \to \bar{\Lambda}\pi^-\Sigma^{*+}$, $\bar{\Lambda} \to \bar{p}\pi^+$, $\Sigma^{*+} \to \pi^+\Sigma^0$, $\Sigma^0 \to \gamma\Lambda$, $\Lambda \to \pi^- p$,	$\psi(3686) \to \gamma\gamma p\pi^+\pi^+\pi^-\pi^-\bar{p}$	21	1	305
22	$\psi(3686) \to \gamma\chi_{c2}$, $\chi_{c2} \to \bar{\Lambda}\rho^0\Sigma^0$, $\bar{\Lambda} \to \bar{p}\pi^+$, $\rho^0 \to \pi^-\pi^+$, $\Sigma^0 \to \gamma\Lambda$, $\Lambda \to \pi^- p$,	$\psi(3686) \to \gamma\gamma p\pi^+\pi^+\pi^-\pi^-\bar{p}$	22	1	306
23	$\psi(3686) \to \gamma\chi_{c1}$, $\chi_{c1} \to \bar{\Sigma}^0\pi^-\Sigma^{*+}$, $\bar{\Sigma}^0 \to \bar{\Lambda}\gamma$, $\Sigma^{*+} \to \pi^+\Lambda$, $\Lambda \to \pi^- p$, $\bar{\Lambda} \to \bar{p}\pi^+$,	$\psi(3686) \to \gamma\gamma p\pi^+\pi^+\pi^-\pi^-\bar{p}$	7	1	307
24	$\psi(3686) \to \pi^-\pi^+ J/\psi$, $J/\psi \to \bar{\Sigma}^{*0}\Lambda$, $\bar{\Sigma}^{*0} \to \bar{\Lambda}\pi^0$, $\Lambda \to \pi^- p$, $\bar{\Lambda} \to \bar{p}\pi^+$,	$\psi(3686) \to \gamma\gamma p\pi^+\pi^+\pi^-\pi^-\bar{p}$	24	1	308
25	$\psi(3686) \to \gamma\chi_{c2}$, $\chi_{c2} \to \bar{\Sigma}^{*-}\pi^+\Sigma^0$, $\bar{\Sigma}^{*-} \to \bar{\Lambda}\pi^-\gamma_{FSR}$, $\Sigma^0 \to \gamma\Lambda$, $\Lambda \to \pi^- p$, $\bar{\Lambda} \to \bar{p}\pi^+$,	$\psi(3686) \to \gamma\gamma\gamma_{FSR} p\pi^+\pi^+\pi^-\pi^-\bar{p}$	25	1	309
26	$\psi(3686) \to \gamma\chi_{c0}$, $\chi_{c0} \to \bar{p}K^{*+}\Lambda$, $K^{*+} \to \pi^+K^0$, $\Lambda \to \pi^- p$, $K^0 \to K_S$, $K_S \to \pi^-\pi^+$,	$\psi(3686) \to \gamma p\pi^+\pi^+\pi^-\pi^-\bar{p}$	8	1	310
27	$\psi(3686) \to \eta J/\psi$, $\eta \to \pi^-\gamma\pi^+$, $J/\psi \to \bar{\Lambda}\gamma\Lambda$, $\bar{\Lambda} \to \bar{p}\pi^+$, $\Lambda \to \pi^- p$,	$\psi(3686) \to \gamma\gamma p\pi^+\pi^+\pi^-\pi^-\bar{p}$	27	1	311
28	$\psi(3686) \to \pi^-\pi^+ J/\psi$, $J/\psi \to \bar{\Lambda}\Sigma^{*0}$, $\bar{\Lambda} \to \bar{p}\pi^+$, $\Sigma^{*0} \to \pi^0\Lambda$, $\Lambda \to \pi^- p$,	$\psi(3686) \to \gamma\gamma p\pi^+\pi^+\pi^-\pi^-\bar{p}$	9	1	312
29	$\psi(3686) \to \gamma\chi_{c1}$, $\chi_{c1} \to \bar{\Sigma}^0\pi^+\Sigma^{*-}$, $\bar{\Sigma}^0 \to \bar{\Lambda}\gamma$, $\Sigma^{*-} \to \pi^-\Lambda$, $\Lambda \to \pi^- p$, $\bar{\Lambda} \to \bar{p}\pi^+$,	$\psi(3686) \to \gamma\gamma p\pi^+\pi^+\pi^-\pi^-\bar{p}$	15	1	313
30	$\psi(3686) \to \pi^-\pi^+ J/\psi$, $J/\psi \to \bar{\Delta}^0\pi^-\Delta^+$, $\bar{\Delta}^0 \to \bar{p}\pi^+$, $\Delta^+ \to \pi^0 p$,	$\psi(3686) \to \gamma\gamma p\pi^+\pi^+\pi^-\pi^-\bar{p}$	16	1	314
31	$\psi(3686) \to \pi^-\pi^+ J/\psi$, $J/\psi \to \bar{\Lambda}\pi^0\Lambda$, $\bar{\Lambda} \to \bar{p}\pi^+$, $\Lambda \to \pi^- p$,	$\psi(3686) \to \gamma\gamma p\pi^+\pi^+\pi^-\pi^-\bar{p}$	31	1	315
32	$\psi(3686) \to \bar{\Lambda}\rho^0\Sigma^{*0}$, $\bar{\Lambda} \to \bar{p}\pi^+$, $\rho^0 \to \pi^-\pi^+$, $\Sigma^{*0} \to \pi^0\Lambda$, $\Lambda \to \pi^- p$,	$\psi(3686) \to \gamma\gamma p\pi^+\pi^+\pi^-\pi^-\bar{p}$	32	1	316
33	$\psi(3686) \to \pi^0 h_c$, $h_c \to \bar{\Sigma}^{*+}\pi^-\Lambda$, $\bar{\Sigma}^{*+} \to \bar{\Lambda}\pi^+$, $\Lambda \to \pi^- p$, $\bar{\Lambda} \to \bar{p}\pi^+$,	$\psi(3686) \to \gamma\gamma p\pi^+\pi^+\pi^-\pi^-\bar{p}$	33	1	317
34	$\psi(3686) \to \gamma\chi_{c2}$, $\chi_{c2} \to \bar{\Sigma}^{*-}\pi^+\Lambda$, $\bar{\Sigma}^{*-} \to \bar{\Sigma}^0\pi^-$, $\Lambda \to \pi^- p$, $\bar{\Sigma}^0 \to \bar{\Lambda}\gamma$, $\bar{\Lambda} \to \bar{p}\pi^+$,	$\psi(3686) \to \gamma\gamma p\pi^+\pi^+\pi^-\pi^-\bar{p}$	34	1	318

Table 2: Inclusive MC topology

Tab 2 shows the signal channel and the background channel and their contributions of 5×10^8 inclusive Monte Carlo sample within ω mass window after the final event selection criteria. After the above selection requirements, signal and background events are 226 and 100, respectively. And we can find that all of those backgrounds hardly have ω in the final state. So we can use the events in sideband region the ($bluearrow, 0.693\ GeV \sim 0.723\ GeV$ and $0.843\ GeV \sim 0.873\ GeV$) to estimate the backgrounds in the signal region ($redarrow, 0.753\ GeV \sim 0.813\ GeV$) , in Fig. 5 (a).

To study the contribution from electromagnetic process $e^+e^- \to \Lambda\bar{\Lambda}\omega$, we analyzed the continuum data collected at 3.65 GeV. No events pass the selection cuts. We use the data collected at 3.77 GeV instead, assuming the non-DDbar decay of $\psi(3773) \to \Lambda\bar{\Lambda}\omega$ is negligible. Fig. 5 (b) shows the $\psi(3773)$ events within ω mass window after the final event selection criteria and then normalize it to $\psi(3686)$. No significant ω signal can be observed here, so we can ignore the continuous contribution of electromagnetic process $e^+e^- \to \Lambda\bar{\Lambda}\omega$ in the background.

5 Branching fraction measurement

Fig 6 shows the fitting results of the ω signal. Unbinned maximum likelihood method is adopted. The signal probability density function(PDF) is described by a RooKeys PDF of the signal MC and the background is described by a first order Chebychev polynomial.

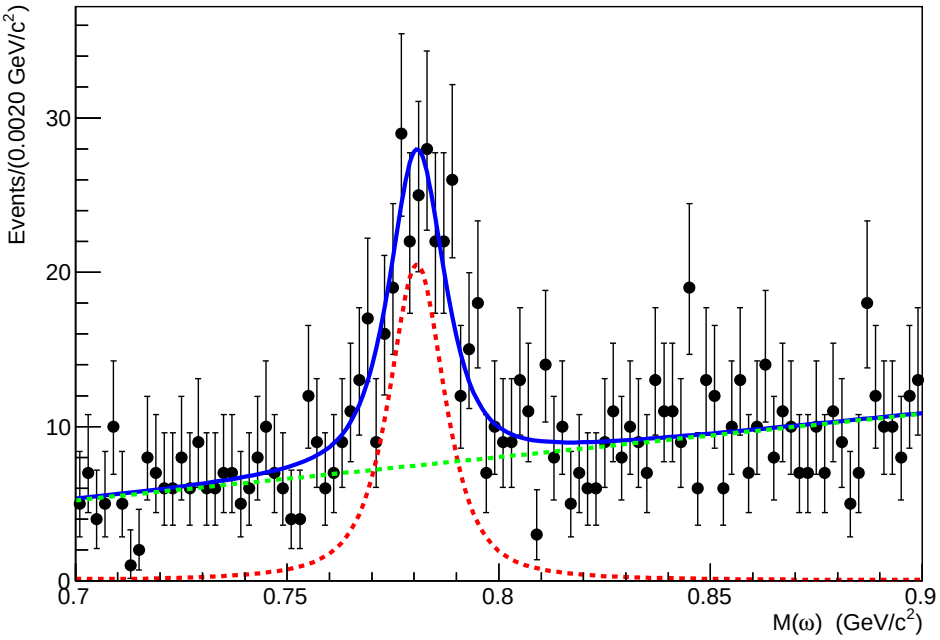

Figure 6: Fitting results of $M_{\pi^+\pi^-\pi^0}$. Dots with error bars are data, the blue curve is the fitting results, the red dotted curve is the omega signal, the green dotted curve is the background pdf.

Branching fraction of $\psi(3686) \to \Lambda\bar{\Lambda}\omega$ can be written as :

$$B(\psi(3686) \to \Lambda\bar{\Lambda}\omega) = \frac{N_{obs}}{N_{\psi(3686)} \times B(\Lambda \to p\pi^-) \times B(\bar{\Lambda} \to \bar{p}\pi^+) \times B(\omega \to \pi^+\pi^-\pi^0) \times B(\pi^0 \to \gamma\gamma) \times \varepsilon}$$

N_{obs} is the number of the observed events, which is yielded by fitting the invariant mass spectrum of ω after the final event selection. $N_{\psi(3686)} = (448 \pm 2.9) \times 10^6$ is the total number of the $\psi(3686)$ events. ε is detection efficiency estimated by MC simulation, which is $(3.79 \pm 0.02)\%$. $B(\Lambda \to p\pi^-)$, $B(\bar{\Lambda} \to \bar{p}\pi^+)$, $B(\omega \to \pi^+\pi^-\pi^0)$ and $B(\pi^0 \to \gamma\gamma)$ are the corresponding decays quoted from PDG[4]. The yield of ω is 209 ± 21. The measurement of $B(\psi(3686) \to \Lambda\bar{\Lambda}\omega)$ is $(3.42 \pm 0.34(stat.)) \times 10^{-5}$. The error is statistical only.

6 Search for $\Lambda^*/\bar{\Lambda}^*$

The invariant mass spectra of $\Lambda\omega$, $\bar{\Lambda}\omega$ and $\Lambda\bar{\Lambda}$ are shown in Fig. 7 (a) (b) (c), respectively. Fig. 7 (d) shows the Dalitz plot of $\psi(3686) \to \Lambda\bar{\Lambda}\omega$. We perform a 2-Dimensional fit to the Dalitz plot of $\psi(3686) \to \Lambda\bar{\Lambda}\omega$.

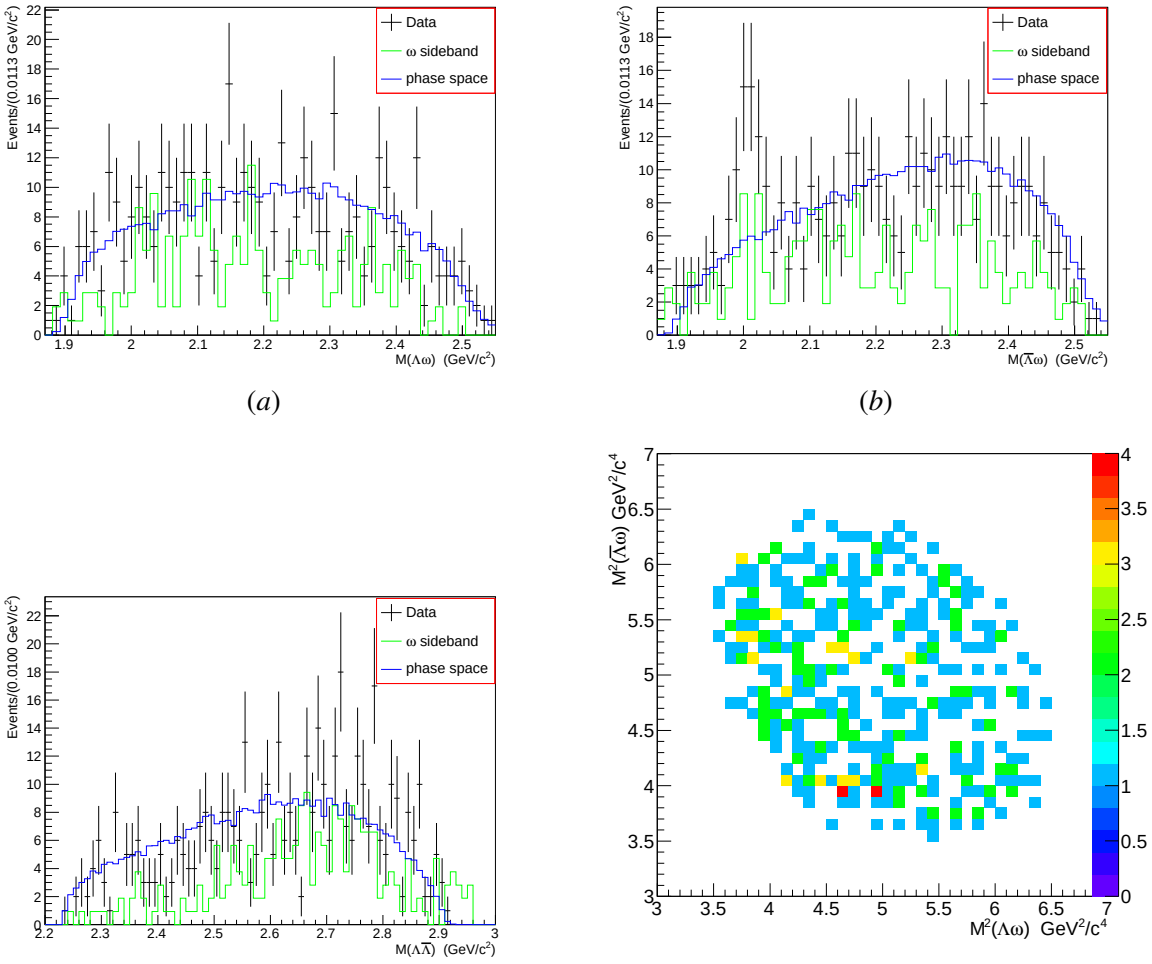

(*a*) (*b*)

(*c*) (*d*)

Figure 7: (a)(b)(c) shows the the invariant mass distribution of $\Lambda\omega$ $\Lambda\omega$ and $\Lambda\bar{\Lambda}$ respectively , The dots with error bars are from $\psi(3686)$ data, green histogram shows the background estimated with the ω sideband, blue histogram shows the phase space MC of $\psi(3686) \to \Lambda\bar{\Lambda}\omega$, which is normalized to data(d) shows the Dalitz plots of $\psi(3686) \to \Lambda\bar{\Lambda}\omega$ from $\psi(3686)$ data

6.1 Signal shape

The Λ^* resonances can be described by a S−Wave Breit−Wigner function. The 2−Dimensional signal PDF can be expressed as:

$$\epsilon(x,y)\cdot\left(\frac{p\cdot q}{(M_R^2-x)^2+M_R^2\cdot\Gamma^2}+\frac{p\cdot q}{(M_R^2-y)^2+M_R^2\cdot\Gamma^2}\right)\otimes\sigma(x,y) \tag{6.1.1}$$

where x, y is the spectra of $M^2(\Lambda\omega)$ and $M^2(\bar{\Lambda}\omega)$, respectively; M_R and Γ are the mass and width of $\Lambda^*/\bar{\Lambda}^*$; p is the momentum of $\Lambda^*/\bar{\Lambda}^*$ in the c.m. frame; q is the momentum of ω in the rest frame of $\Lambda^*/\bar{\Lambda}^*$. The definition of the momentum of particle 1(2) in the rest frame of particle with mass M, which decays into two particles with mass m_1 and m_2 :

$$|p_1|=|p_2|=\frac{\sqrt{(M^2-(m_1+m_2)^2)(M^2-(m_1-m_2)^2)}}{2M} \tag{6.1.2}$$

σ is the Gaussian resolution function for x and y, obtained from a zero width Λ^* and $\bar{\Lambda}^*$ signal MC. The resolution is shown in Fig. 8 (a) .$\epsilon(x,y)$ is the 2−Dimensional detection efficiency of x and y as shown in Fig. 8 (b), which is obtained from $\psi(3686)\to\Lambda\bar{\Lambda}\omega$ exclusive MC.

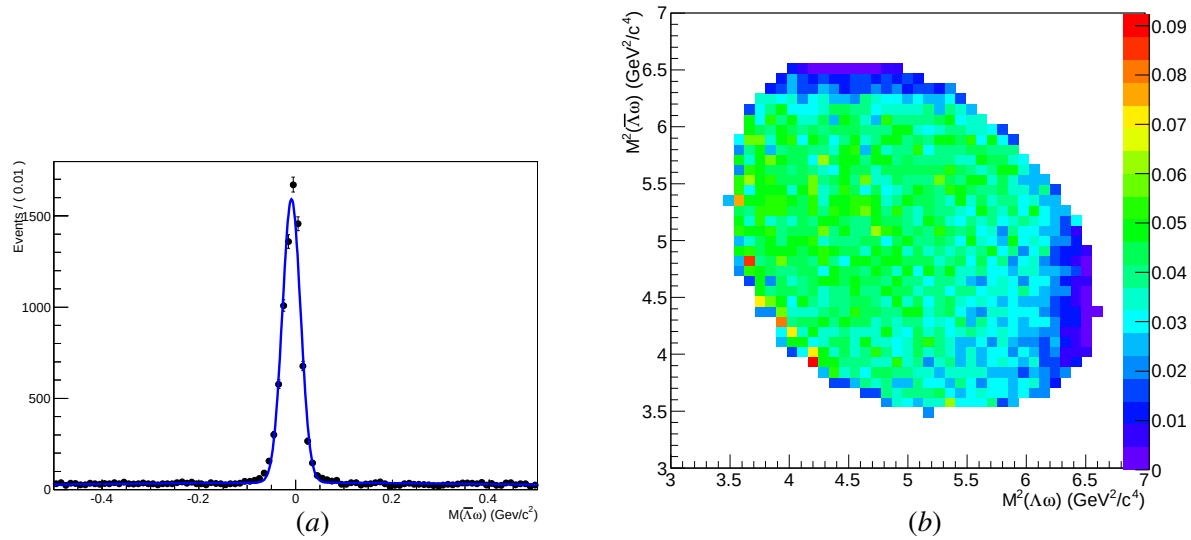

Figure 8: (a) shows resolution function of $\Lambda\omega$ (b) shows 2-detection efficiency of $M^2(\Lambda\omega)$ versus $M^2(\bar{\Lambda}\omega)$

6.2 Background shape

The background can be composed of two parts,

- The non−resonant contribution is described by PHSP MC, which is floating in the fit.

- The non−omega background is described by the normalized ω sidebands, which is fixed in the fit.

6.3 Fitting result of a hypothetical $\Lambda^*/\bar{\Lambda}^*$ resonance

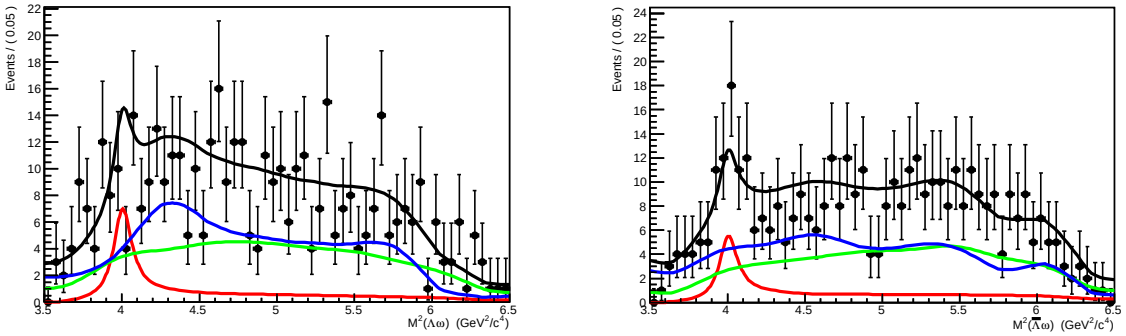

Figure 9: The fitting results of a 2-Dimensional fit to the Dalitz plot of $\psi(3686) \to \Lambda\bar{\Lambda}\omega$. Dots with error bars are data, the black curve is the fitting results, the red curve is the $\Lambda^*/\bar{\Lambda}^*$ signal, the green curve is the ω phase space background pdf and the blue curve is the ω sideband background pdf.

An unbinned maximum likelihood fit is performed to data. The projection of 2-dimensional fitting results is shown in Fig 9, where the the dots represent data, the red dotted line is the signal shape, the green dotted line is the background described by ω sideband and blue line is the background described by PHSP MC. The fitted $\Lambda^*/\bar{\Lambda}^*$ parameters are $M_{\Lambda^*/\bar{\Lambda}^*}$=2.001 ± 0.007 GeV/c^2, $\Gamma_{\Lambda^*/\bar{\Lambda}^*}$=0.036 ± 0.014 GeV/c^2, and the signal yields is 51±16 with a significance of 3.3σ. And the goodness of fit(χ^2/bin) for $M^2_{\Lambda\omega}$ and $M^2_{\bar{\Lambda}\omega}$ is 1.12 and 0.46, respectively.

To validate the fit, we performed various crosschecks as described in the Appendix.

6.4 Upper limit of $\Lambda^*/\bar{\Lambda}^*$

In this analysis, we use a Bayesian method to calculate obtain the upper limit of the branching fraction of $\psi(3686) \to \Lambda\bar{\Lambda}^*/\bar{\Lambda}\Lambda^* \to \Lambda\bar{\Lambda}\omega$. We perform the fit many times with different hypothesis of signal number, and the corresponding normalized likelihood values can be obtained. The upper limit of the signal yields at the 90% confidence level(C. L.) is defined as N_{UL}, corresponding to the number of events at 90% of the integral of the probability density function(PDF).The curve of normalized likelihood value versus number of signal is plotted in Fig 10.

The upper limit branching fractions of $\psi(3686) \to \Lambda\bar{\Lambda}^*/\bar{\Lambda}\Lambda^* \to \Lambda\bar{\Lambda}\omega$ is calculated as follows:

$$B(\psi(3686) \to \Lambda\bar{\Lambda}^*/\bar{\Lambda}\Lambda^* \to \Lambda\bar{\Lambda}\omega) < \frac{N_{UL}}{N_{\psi(3686)} \times B(\Lambda \to p\pi^-) \times B(\bar{\Lambda} \to \bar{p}\pi^+) \times B(\omega \to \pi^+\pi^-\pi^0) \times B(\pi^0 \to \gamma\gamma) \times \varepsilon} \quad (6.4.1)$$

where N_{UL} is the number of the observed signal events extracted from the fit to the daliz plot ($M^2_{\Lambda\omega}$ vs $M^2_{\bar{\Lambda}\omega}$) for the decay mode of $\psi(3686) \to \Lambda\bar{\Lambda}\omega$, $N_{\psi(3686)}$ is the number of $\psi(3686)$[7], ε is the

MC-determined detection efficiency. $B(\Lambda \to p\pi^-), B(\bar{\Lambda} \to \bar{p}\pi^+), B(\omega \to \pi^+\pi^-\pi^0)$ *and* $B(\pi^0 \to \gamma\gamma)$ are the branching fraction of $\Lambda \to p\pi^-, \bar{\Lambda} \to \bar{p}\pi^+, \omega \to \pi^+\pi^-\pi^0$ *and* $\pi^0 \to \gamma\gamma$ quoted from the PDG[10],respectively.

To take into account the systematic uncertainties related to the fits, alternative fits with different ω sideband background level and shape are performed. We study the uncertainty of background level by changing the number of fixed background event by one standard deviation of statistical uncertainty. We study the uncertainty of background shape by varying the region of ω sidebands. The maximum upper limit of the signal yields N_{UL} among these cases is chosen to calculate the upper limit of branching fraction at 90% confidence level. The results for different situations are list in Table3.

	Sideband range	Number of fixed background events	N_{UL}
Original	$[0.693, 0.723]\ GeV, [0.843, 0.873]\ GeV$	226	78.9
Background level	$[0.693, 0.723]\ GeV, [0.843, 0.873]\ GeV$	217	79.8
	$[0.693, 0.723]\ GeV, [0.843, 0.873]\ GeV$	234	78.2
Background shape	$[0.688, 0.718]\ GeV, [0.838, 0.868]\ GeV$	226	68.8
	$[0.698, 0.728]\ GeV, [0.848, 0.878]\ GeV$	226	69.6

Table 3: Different method for the the upper limit of branching of $Br(\psi(3686) \to \Lambda\bar{\Lambda}^*/\bar{\Lambda}\Lambda^* \to \Lambda\bar{\Lambda}\omega)$

From Table3, the maximum number of signal is 79.8. The upper limit branching fraction is calculated to be $Br(\psi(3686) \to \Lambda\bar{\Lambda}^*/\bar{\Lambda}\Lambda^* \to \Lambda\bar{\Lambda}\omega) < 1.93 \times 10^{-5}$.

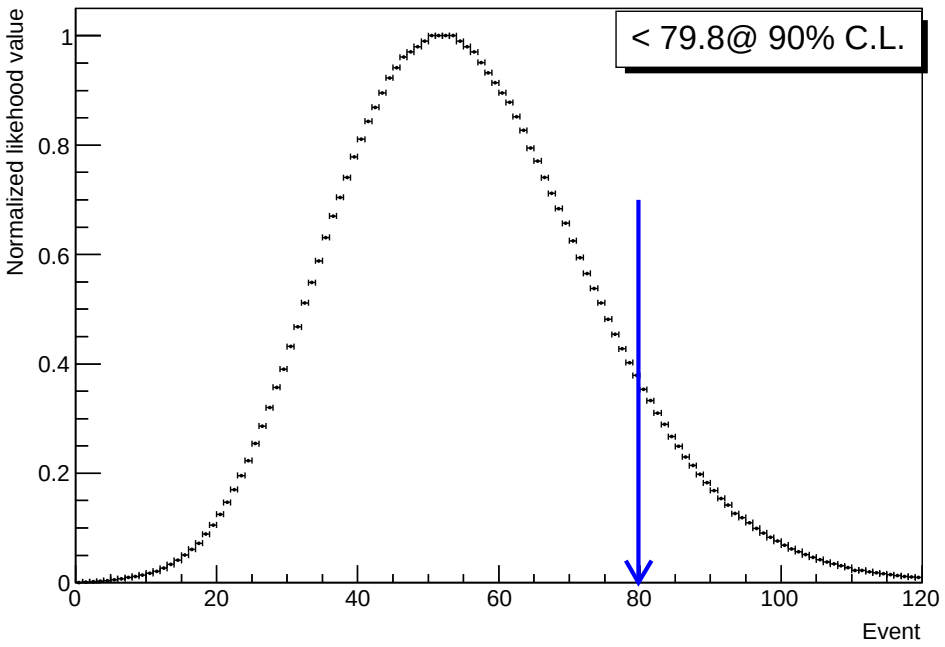

Figure 10: The curve of Normalized likelihood value versus number of signal

7 Systematic uncertainties

- $\psi(3686)$ total number. The uncertainty due to the number of $\psi(3686)$ events is 0.65%.[10]

- MDC tracking and PID efficiency. The uncertainty of the tracking efficiency is taken to be 1.0% per track, and we take 6.0% for total uncertainty of tracking efficiency in our analysis. The average PID efficiency difference between data and MC is 2.0% per charged particle and %4.0 is taken as the systematic uncertainty for two charged tracks to reconstruct π^0.[11][12]

- $\Lambda/\bar{\Lambda}$ and π^0 reconstruction. The $\Lambda/\bar{\Lambda}$ reconstruction have been studied in the decay $\psi(3686) \to \Lambda\bar{\Lambda}\eta$, which has same final state of $\psi(3686) \to \Lambda\bar{\Lambda}\omega$[13]. In this study we take 2.0% as $\Lambda/\bar{\Lambda}$ reconstruction.The uncertainty of the π^0 reconstruction from $\gamma\gamma$ final state is 1.0% per π^0, which is determined from a high purity control sample of $J/\psi \to p\bar{p}\pi^0$.[14]

- Photon detection efficiency. The uncertainty in the photon reconstruction is studied by using the control sample $J/\psi \to \rho^0\pi^0$, and a 1.0% systematic uncertainty is estimated for each photon.[15] As there are two photons in the decay final state of $\psi(3686) \to \Lambda\bar{\Lambda}\omega$, the photon detection efficiency is determined to be 2.0%.

- Kinematic Fit. The systematic uncertainty due to kinematic fitting is estimated by correcting the helix parameters of charged tracks according the method described in Ref.[12]. Difference in thetection efficiency between with and without correction to the MC samples is taken as the uncertainty.

- Intermediate decay. The systematic uncertainties on the intermediate-decay $\Lambda \to p\pi^-$, $\bar{\Lambda} \to \bar{p}\pi^+$, $\omega \to \pi^+\pi^-\pi^0$ and $\pi^0 \to \gamma\gamma$ are quoted from PDG[4].

- Mass window. The systematic error of ($M_{p\pi^-}$, $M_{\bar{p}\pi^+}$,and $M_{\pi^+\pi^-\pi^0}$) mass window cut is due to the different mass resolution of them between data and signal MC. We use a gauss function smear the signal MC shape to get a better consistent with data, and the difference of the MC detection efficiency before and after smear is taken as the systematic uncertainties from this item. The uncertainty from J/ψ veto is estimated by varying the mass window cut, the alternative fit with different J/ψ mass window is performed.

- Fitting

  For the measurements of $\psi(3686) \to \Lambda\bar{\Lambda}\omega$ branching fraction .

  a. Signal shape

The signal shape in measure branching fraction of $\psi(3686) \to \Lambda\bar{\Lambda}\omega$ is described by a RooKeys PDF of the signal MC. A fit is performed by useing a RooKeys PDF of the signal MC convolutes a Gaussian function as the signal pdf and take the different as the systematic error, which is 2.9 percent

b. Background shape

The description of backgrounds in measure branching fraction of $\psi(3686) \to \Lambda\bar{\Lambda}\omega$ is described by a first order Chebyshev polynomial. There is a second order Chebyshev polynomial as the background pdf and take the different as the systematic error, which is 1.4 percent

c. Fitting range

Changing the fit range and taking the difference as the uncertainty which is 1.5 percent.

Tab 4 demonstrates the possible systematic error sources and their fractional contribution to the measurement of $\psi(3686) \to \Lambda\bar{\Lambda}\omega$ branching fraction and upper limit of $\Lambda^*/\bar{\Lambda}^*$.

soure		$\psi(3686) \to \Lambda\bar{\Lambda}\omega$	Upper limit of $\Lambda^*/\bar{\Lambda}^*$
Number of $\psi(3686)$ events		0.65%	0.65%
MDC tracking		6%	6%
PID		4%	4%
$\Lambda/\bar{\Lambda}$ reconstruction		2%	2%
π^0 reconstruction		1%	1%
Good photon		2%	2%
Kinematic Fit		1.7%	1.7%
Intermediate decay	$\Lambda \to p\pi^-$	0.8%	0.8%
	$\bar{\Lambda} \to \bar{p}\pi^+$	0.8%	0.8%
	$\omega \to \pi^+\pi^-\pi^0$	0.8%	0.8%
	$\pi^0 \to \gamma\gamma$	0.03%	0.03%
Mass window	$\lvert M_\Lambda - m_\Lambda \rvert < 5\ MeV/c^2$	0.02%	0.04%
	$\lvert M_{\bar{\Lambda}} - m_{\bar{\Lambda}} \rvert < 5\ MeV/c^2$	0.03%	0.02%
	$\lvert M^{rec}_{\pi^+\pi^-} - m_{J/\psi} \rvert > 30\ MeV/c^2$	1.6%	1.8%
	$\lvert M_\omega - m_\omega \rvert < 30\ MeV/c^2$	$---$	0.02%
Fitting	Signal shape	2.9%	$---$
	Background shape	1.4%	$---$
	Fitting range	1.5%	$---$
Total		9.1%	8.3%

Table 4: Summary of systematic uncertainties

7.1 Result

The branching fraction of $\psi(3686) \to \Lambda\bar{\Lambda}\omega$ is $(3.42 \pm 0.34(stat.) \pm 0.31(syst.)) \times 10^{-5}$.

To conservatively estimate the upper limit of branching fractions, the multiplicative uncertainties are considered by smearing the normalized likelihood curve with a Gaussian function $G(\mu, \sigma) = G(0, \sigma_{sys})$,

$\sigma_{sys} = N * \sigma_{rel}$, $\sigma_{rel}(= 8.3\%)$ is the corresponding combined relativity uncertainty and N is the input signal yield:

$$L(N^{'}) = \int_0^{\infty} L(N) \frac{1}{\sqrt[2]{2\pi}\sigma_{sys}} exp[-\frac{(N^{'} - N)^2}{2\sigma_{sys}^2}]dN \tag{7.1.1}$$

where L(N) is the normalized likelihood distribution obtained from fitting the curve of normalized likelihood value vs signal number and parameterized as a Gaussian function.

The Fig **??** shows the likelihood distribution before and after smearing. In this way, the upper limit of the branching fraction at the 90% confidence level is determined to be 1.93×10^{-5}

8 Summary

Using a sample of 4.48×10^8 $\psi(3686)$ events collected with BESIII detector at BEPCII storage ring taken in the year 2009 and 2012, at center-of-mass energy $\sqrt{s} = 3.686\ GeV/c^2$, the measurement of $\psi(3686) \to \Lambda\bar{\Lambda}\omega$ is analyzed, which is observed for the first time, and the branching fraction of $\psi(3686) \to \Lambda\bar{\Lambda}\omega$ is measured to be $(3.42 \pm 0.34(stat.) \pm 0.31(syst.)) \times 10^{-5}$. A search for the decay $\psi(3686) \to \bar{\Lambda}^*\Lambda/\Lambda^*\bar{\Lambda} \to \Lambda\bar{\Lambda}\omega$ is performed via the process $\psi(3686) \to \Lambda\bar{\Lambda}\omega$. There is no evidence of any Λ^* in both and mass distributions. However a 2-dimesional fit to the Dalitz plot of $\psi(3686) \to \Lambda\bar{\Lambda}\omega$ gives a mass of $2.001 \pm 0.007\ GeV/c^2$ and width is $0.036 \pm 0.014\ GeV/c^2$ with the significance of 3.3σ. The corresponding upper limit of $Br(\psi(3686) \to \bar{\Lambda}^*\Lambda/\Lambda^*\bar{\Lambda} \to \Lambda\bar{\Lambda}\omega)$ is measured as 1.93×10^{-5} at C.L. of 90%.

References

[1] J. Beringer et al. [Particle Data Group Collaboration], Review of Particle Physics (RPP), Phys. Rev. D 86, 010001 (2012).

[2] S. Capstick, S. Dytman, R. Holt, X. -d. Ji, J. W. Negele, E. Swanson, P. Barnes and T. Barnes et al.,Key issues in hadronic physics, [hep-ph/0012238].E. Klempt and J. -M. Richard, Baryon spectroscopy, Rev. Mod. Phys. 82,1095 (2010).

[3] B. -S. Zou,N*, Lambda*, Sigma* and Xi* resonances from J / Psi and Psi-prime decays, Nucl.Phys. A 684,330(2001).

[4] M. Tanabashi et al. (Particle Data Group), Phys. Rev. D 98, 030001 (2018).

[5] M. Ablikim et al. (BES Collaboration), Nucl. Instrum. Methods Phys. Res. Sect. A 614, 345 (2010).

[6] S. Agostinelli et al. (GEANT4 Collaboration), Nucl. Instrum. Methods Phys. Res. Sect. A 506, 250 (2003).

[7] S. Jadach, B. Ward, and Z. Was, Phys. Rev. D 63, 113009 (2001).

[8] D. J. Lange, Nucl. Instrum. Methods Phys. Res. Sect. A 462, 152 (2001).

[9] J. C. Chen, G. S. Huang, X. R. Qi, D. H. Zhang, and Y. S. Zhu, Phys. Rev. D 62, 034003 (2000).

[10] M. Ablikim et al. (BES Collaboration), arXiv:1709,03653.

[11] M. Ablikim et al. (BES Collaboration), Phys.Rev.D 87, 012007 (2013)

[12] M. Ablikim et al. (BES Collaboration), Phys.Rev.D 87, 012002 (2013).

[13] M. Ablikim et al. (BES Collaboration), Phys.Rev.D 87,052007 (2013).

[14] M. Ablikim et al. (BES Collaboration), Phys.Rev.Lett.105,261801 (2010).

[15] M. Ablikim et al. (BES Collaboration), Phys.Rev.D 81,052005 (2010).

9 Appendices

9.1 Check the event selection analysis program

Use the branching fraction of $\psi(3686) \to \Lambda\bar{\Lambda}\eta$ to check the event selection analysis program. Fig 11 shows the fitting results of the η signal. Unbinned maximum likelihood method is adopted. The signal probability density function(PDF) is described by a RooKeys PDF of the signal MC and the background is described by a first order Chebychev polynomial, and the detection efficiency estimated by MC simulation is $(2.90\pm0.04)\%$. The yield of η is 28.8 ± 6.4. Thus, the measurement of $B(\psi(3686) \to \Lambda\bar{\Lambda}\eta)$ is $(2.40\pm0.53(stat.))\times10^{-5}$. The error is statistical only. And the branching fraction of $\psi(3686) \to \Lambda\bar{\Lambda}\eta$ is consistent with the branch ratio on PDG within the error range, which is $(2.5 \pm 0.4)) \times 10^{-5}$.

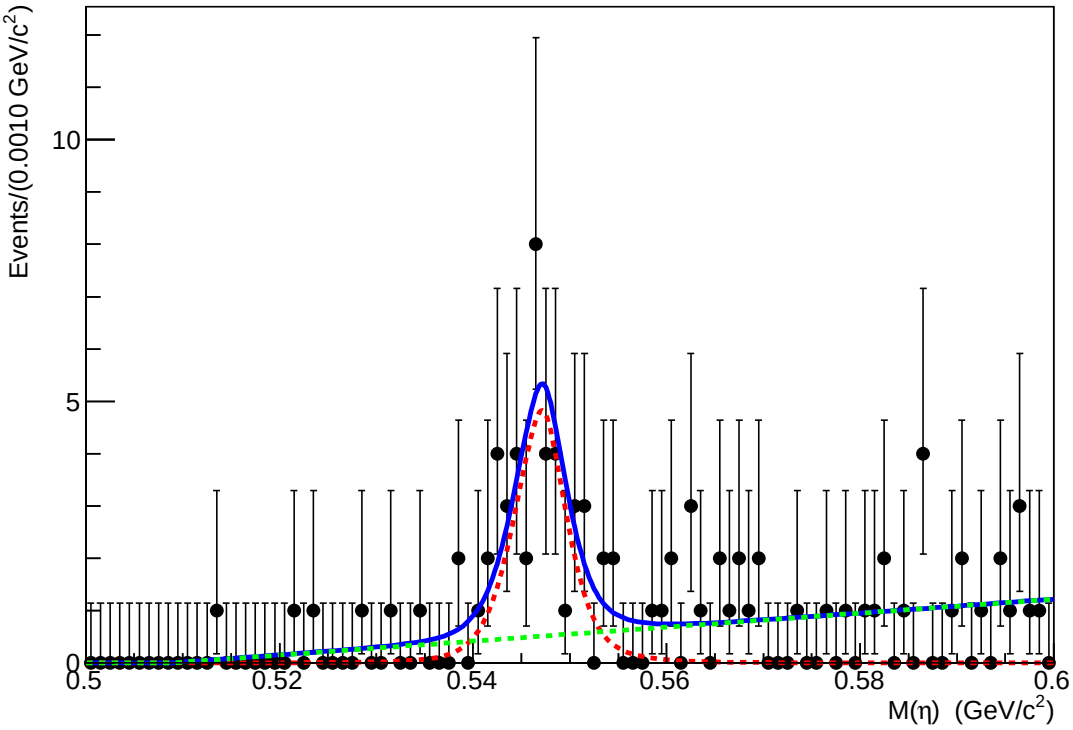

Figure 11: Fitting results of M_η. Dots with error bars are data, the blue curve is the fitting results, the red dotted curve is the omega signal, the green dotted curve is the background pdf.

9.2 The contribution from electromagnetic

To study the contribution from electromagnetic process $e^+e^- \to \Lambda\bar{\Lambda}\omega$, we analyzed the continuum data collected at 3.686GeV. There is no survival events. We use the data collected at 3.773GeV instead, assuming the non-DDbar decay of $\psi(3773) \to \Lambda\bar{\Lambda}\omega$ is negligible . The number of background events

can be normalized using the following formula,

$$N_{QED} = \frac{Lum_{3.686GeV}}{Lum_{3.773GeV}} \times \frac{3.686^2}{3.773^2} \times N_{3.773GeV}$$

where $Lum_{3.686GeV} = 673.98pb^{-1}$, $Lum_{3.773GeV} = 2931.8pb^{-1}$, $N_{3.773GeV}$ is the signal number selected from continuum data which is 16.3 ± 6.3. The corresponding events after normalization with above formula is 3.9 ± 1.5. And there seems no significant ω signals here, so we can ignore the continuous contribution of electromagnetic process $e^+e^- \to \Lambda\bar{\Lambda}\omega$ in the background.

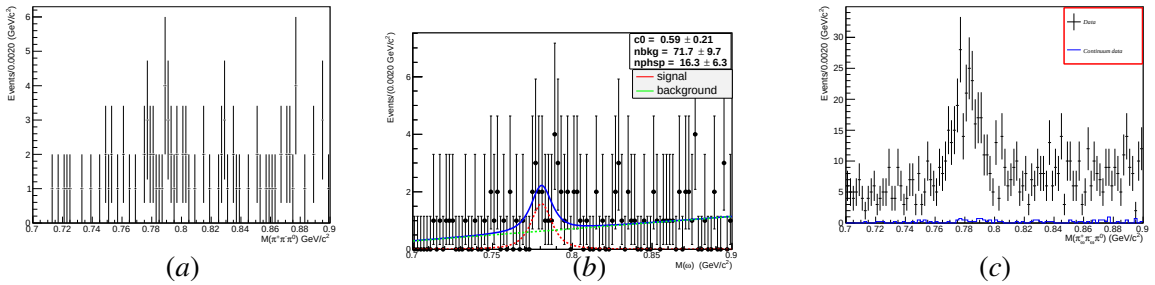

(a) (b) (c)

Figure 12: The $\pi^+\pi^-\pi^0$ invariant mass spectrum.(a) comes from the continuum data at 3.773 GeV before normalization;(b)shows the fitting results of ω invariant mass spectrum at 3.773 GeV, and the yield of ω is 16.3 ± 6.3 and the significance is 2.43σ;(c)shows the difference between data and continuum data at 3.686 GeV, the dots with error bars are from $\psi(3686)$ data, blue histogram shows the background estimated with the continuum data at 3.773 GeV data after the normalization

9.3 Scan of mass and width of $\Lambda^*\bar{\Lambda}^*$

There is the scan of mass and width of $\Lambda^*\bar{\Lambda}^*$. The initial mass value is set to be 1.8 GeV/c^2 and step length is 0.010 GeV/c^2 and the preliminary width is 0.005 GeV/c^2 and the step size is 0.005 GeV/c^2 in the scan. The change likelihood-value versus mass and width plot is shown in Fig 13. From those figure, we can get that the mass of $\Lambda^*/\bar{\Lambda}^*$ is 2.0 GeV/c^2, width is 0.035 GeV/c^2 and they are consistent with the up fitting results.

9.4 Input/output check

There is a weak signal in Section 6.3, and now now 10000 toyMC samples are generated according to the updated fitting results. The 14 is one of fitting results of a 2-Dimensional fit to the Dalitz plot of one of 10000 toyMC samples. The 15 is the pull distribution of the signal yields. By comparison ,The outputs are consistent with the inputs.

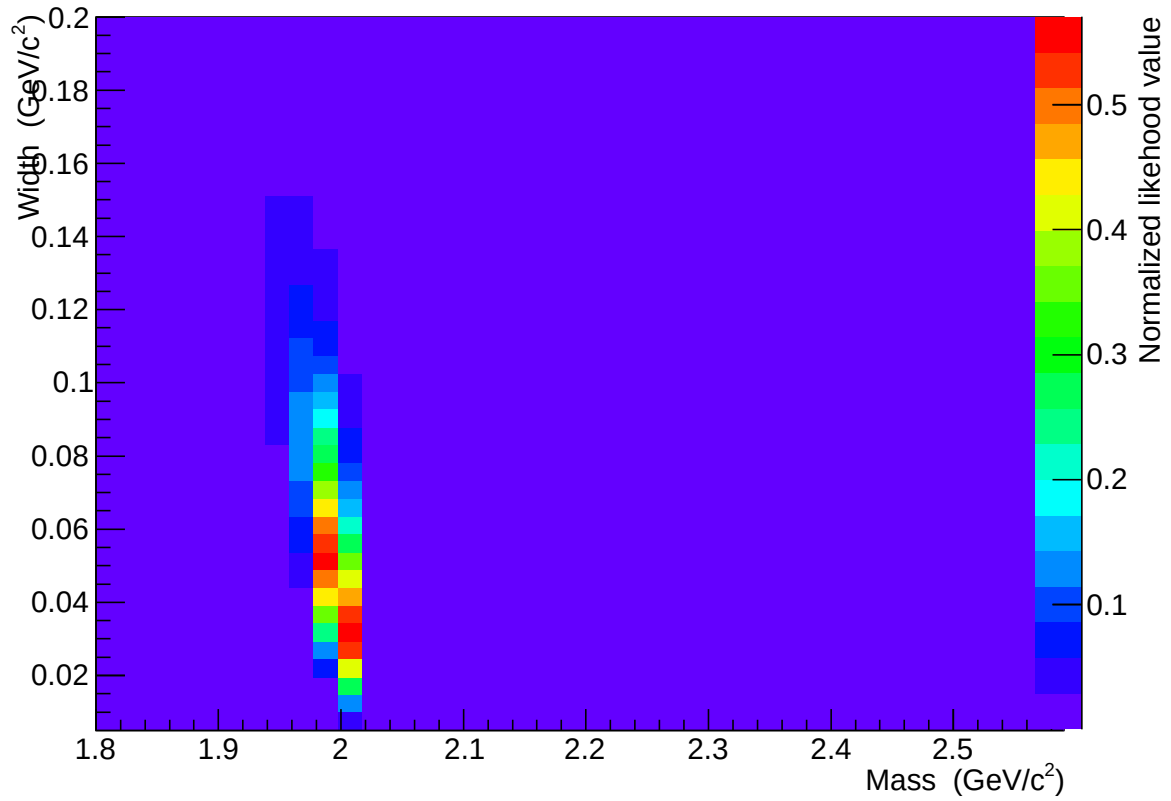

Figure 13: The change likelihood-value versus mass and width plot

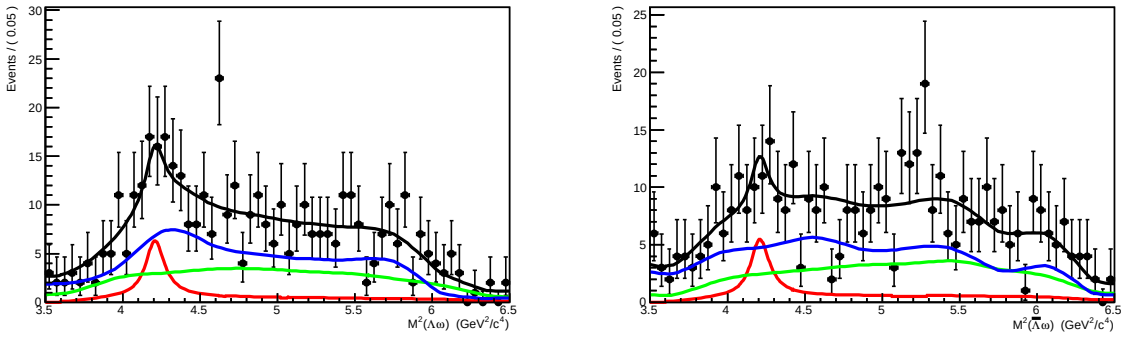

Figure 14: The fitting results of a 2-Dimensional fit to the Dalitz plot of one of 10000 toyMC samples. Dots with error bars are data, the black curve is the fitting results, the red curve is the $\Lambda^*/\bar{\Lambda}^*$ signal, the green curve is the ω phase space background pdf and the blue curve is the ω sideband background pdf. The fitted $\Lambda^*/\bar{\Lambda}^*$ parameters are $M_{\Lambda^*/\bar{\Lambda}^*}$=2.0051 ± 0.009 GeV/c^2, $\Gamma_{\Lambda^*/\bar{\Lambda}^*}$=0.036 ± 0.017 GeV/c^2, and the signal yields is 47 ± 17.

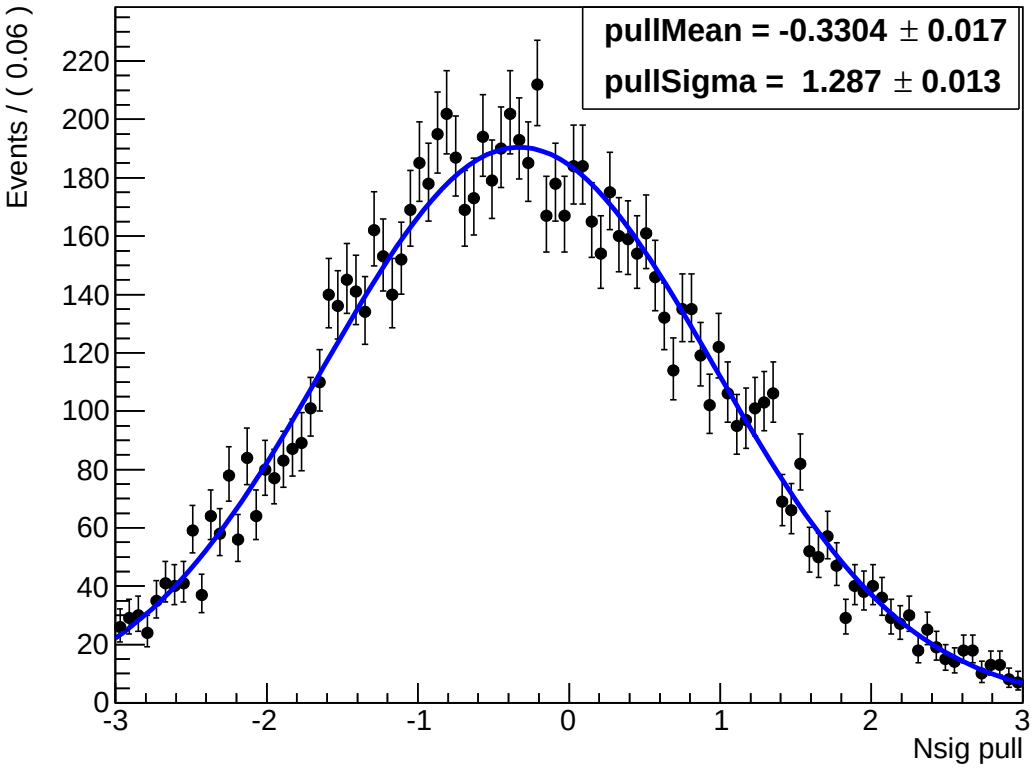

Figure 15: The pull distribution of the signal yields

9.5 J/ψ veto

In order to clarify whether the peak in the $\Lambda\omega$ and $\bar{\Lambda}\omega$ invariant mass spectrum is a signal or a statistical fluctuation. We drew some $\Lambda\omega$ and $\bar{\Lambda}\omega$ invariant mass spectrums with different cuts and compared them.

By comparing these figures, we come to the following conclusions:1) There is no peak background in the $\Lambda\omega$ and $\bar{\Lambda}\omega$ invariant mass spectrum, which is from $\psi(3686) \to \Lambda\bar{\Lambda}\omega$ inclusive MC, regardless of the J/ψ veto cut. 2) If there is a $\Lambda^*/\bar{\Lambda}^*$ signal, there should be a peak on both the $\Lambda\omega$ and $\bar{\Lambda}\omega$ invariant mass spectrum, not $\Lambda\omega$ invariant mass spectrum without a peak, $\bar{\Lambda}\omega$ invariant mass spectrum with a peak.3)When the J/ψ veto cut condition is narrow, there is a peak in the $\bar{\Lambda}\omega$ invariant mass spectrum form data, when the J/ψ veto cut condition is wide, there is no peak. And the peak in the $\bar{\Lambda}\omega$ invariant mass spectrum with the J/ψ veto is 30MeV should be a statistical fluctuation.

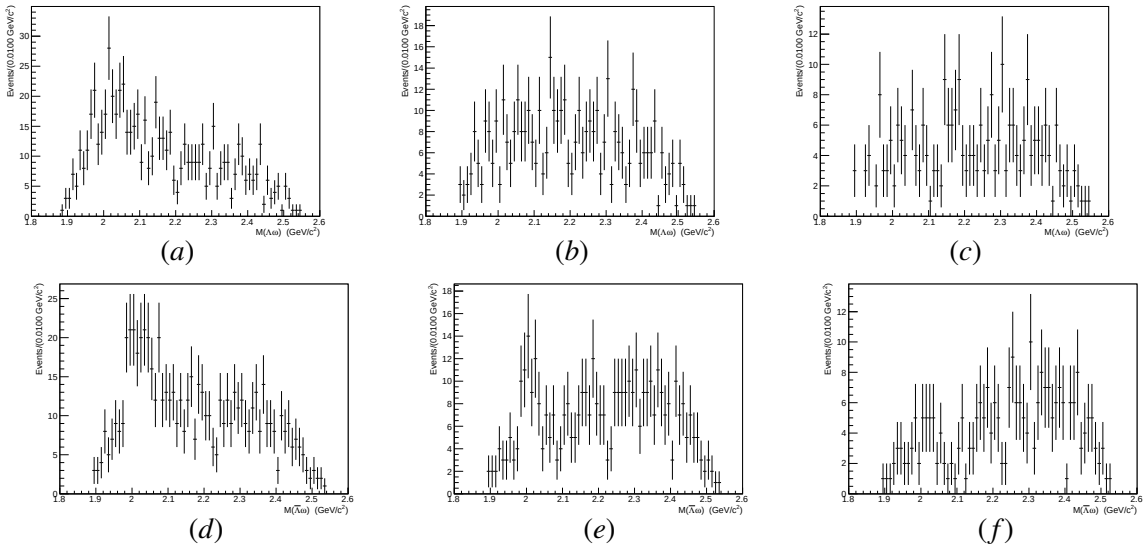

Figure 16: The invariant mass distribution of $\Lambda\omega$ and $\bar{\Lambda}\omega$ from data (a)(d) shows invariant mass distribution of $\Lambda\omega$ and $\bar{\Lambda}\omega$ before J/ψ veto. (b)(e) shows the $\Lambda\omega$ and $\bar{\Lambda}\omega$ invariant mass distribution with $\mid M(J/\psi) - 3.097) \mid > 30MeV$ (c)(f) shows the $\Lambda\omega$ and $\bar{\Lambda}\omega$ invariant mass distribution with $\mid M(J/\psi) - 3.097) \mid > 100MeV$

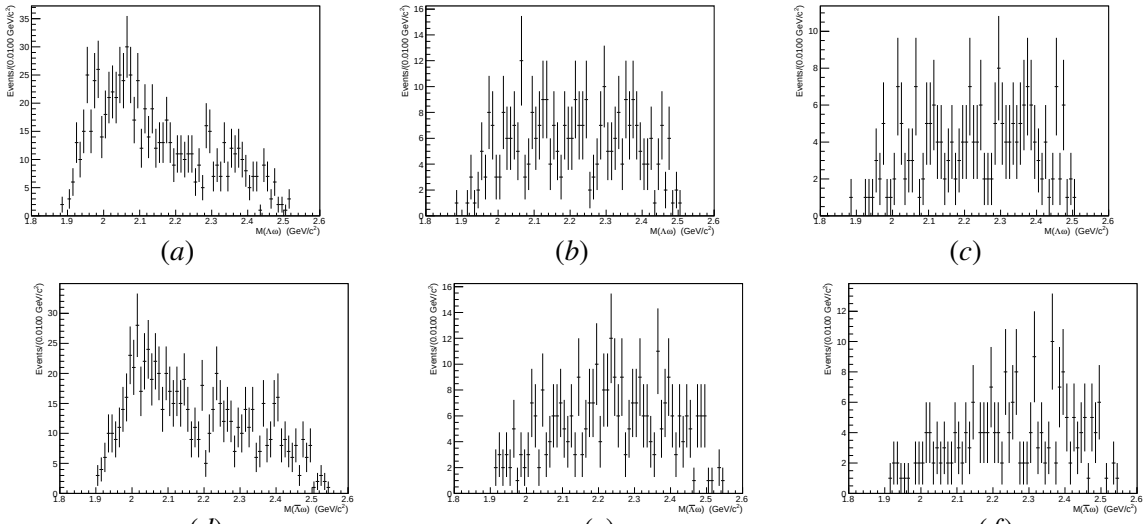

Figure 17: The invariant mass distribution of $\Lambda\omega$ and $\bar{\Lambda}\omega$ from $\psi(3686) \rightarrow \Lambda\bar{\Lambda}\omega$ inclusive MC (a)(d) shows invariant mass distribution of $\Lambda\omega$ and $\bar{\Lambda}\omega$ before J/ψ veto. (b)(e) shows the $\Lambda\omega$ and $\bar{\Lambda}\omega$ invariant mass distribution with $\mid M(J/\psi) - 3.097) \mid > 30MeV$ (c)(f) shows the $\Lambda\omega$ and $\bar{\Lambda}\omega$ invariant mass distribution with $\mid M(J/\psi) - 3.097) \mid > 100MeV$

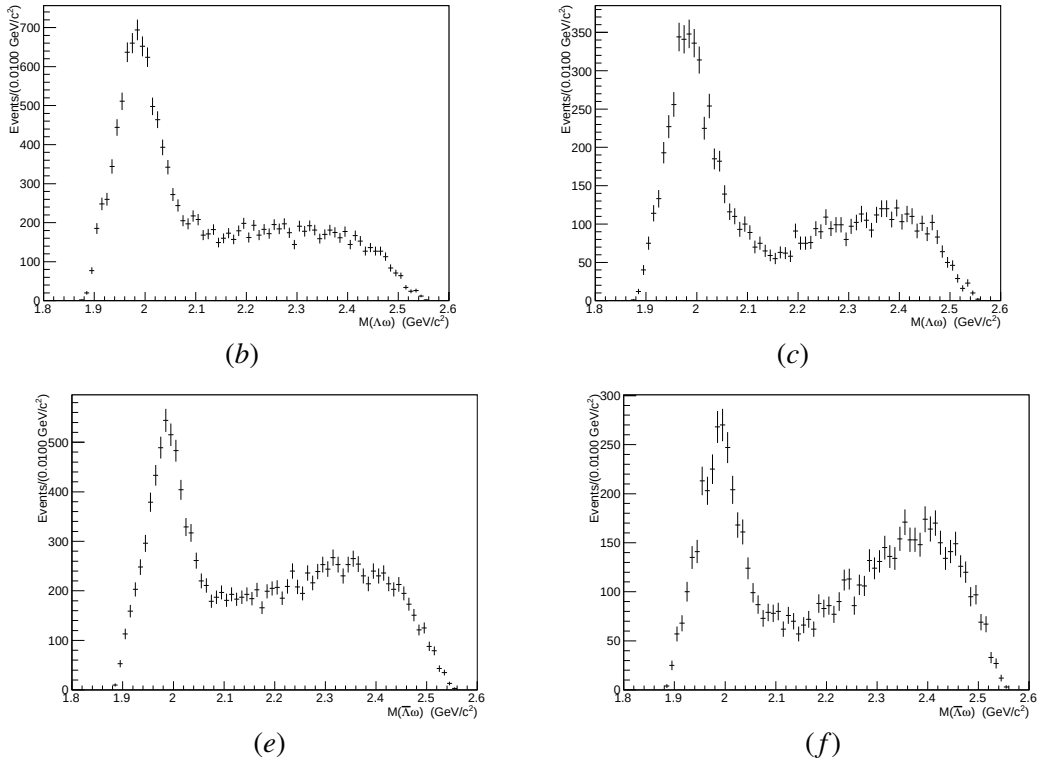

Figure 18: The invariant mass distribution of $\Lambda\omega$ and $\bar{\Lambda}\omega$ from $\psi(3686) \rightarrow \Lambda\bar{\Lambda}^*/\Lambda^*\bar{\Lambda}(Mean = 2.0GeV\ Width = 100MeV) \rightarrow \Lambda\bar{\Lambda}\omega$ exclusive MC (a)(c) shows the $\Lambda\omega$ and $\bar{\Lambda}\omega$ invariant mass distribution with $\mid M(J/\psi) - 3.097) \mid > 30MeV$ (b)(d) shows the $\Lambda\omega$ and $\bar{\Lambda}\omega$ invariant mass distribution with $\mid M(J/\psi) - 3.097) \mid > 100MeV$